

---

# Known By Their Actions: Fingerprinting LLM Browser Agents via UI Traces

---

William Lugoloobi<sup>1\*</sup> Samuelle Marro<sup>2</sup> Jabez Magomere<sup>1</sup> Joss Wright<sup>1</sup> Chris Russell<sup>1</sup>

<sup>1</sup>Oxford Internet Institute, University of Oxford

<sup>2</sup>Department of Engineering Science, University of Oxford

## Abstract

As LLM-based agents increasingly browse the web on users' behalf, a natural question arises: can websites passively identify which underlying model powers an agent? Doing so would represent a significant security risk, enabling targeted attacks tailored to known model vulnerabilities. Across 14 frontier LLMs and four web environments spanning information retrieval and shopping tasks, we show that an agent's actions and interaction timings, captured via a passive JavaScript tracker, are sufficient to identify the underlying model with up to 96% F1. We formalise this attack surface by demonstrating that classifiers trained on agent actions generalise across model sizes and families. We further show that strong classifiers can be trained from few interaction traces and that agent identity can be inferred early within an episode. Injecting randomised timing delays between actions substantially degrades classifier performance, but does not provide robust protection: a classifier retrained on delayed traces largely recovers performance. We release our harness and a labelled corpus of agent traces here.

## 1 Introduction

LLM-based agents that browse the web and operate computer interfaces on behalf of users are moving rapidly from research prototypes to production [1–3]. As these systems are deployed at scale across live websites, every page they visit becomes a potential observation point, and we show that observation alone is enough to identify the model. This exposes users to potential security risks.

Every agent visit to a website leaves a trace of clicks, scrolls, keypresses, and other *actions* observable to any party controlling the page. Prior work has established that behavioural traces like this distinguish human users from automated clients [4, 5], and that passively collected browser attributes re-identify human users across sessions [6, 7]. These works ask a binary question: human or bot. As LLM-based agents displace scripted automation, we probe deeper: *given that the client is an agent, which model is pulling the strings?* In classical security frameworks, target identification is the first step toward exploitation [8]. Thus for LLM-based agents, knowing the underlying model enables more targeted attacks: an adversary can select from a known set of model-specific jailbreaks or reduce the search space for a white-box adversarial attack [9].

To our knowledge, we are the first to show that the underlying foundation model of a browser agent can be inferred from passive in-page UI traces alone. Using lightweight classifiers trained on UI action traces collected via injected JavaScript, we achieve agent identification F1's of up to 96% across 14 frontier LLMs. The identification does not rely on browser attributes and headers (which can be spoofed), but on the temporal and structural dynamics of how different models navigate, click, and interact with page elements. In other words, the behaviour of a model is sufficient to accurately identify it. For adversaries, this means that agents can be identified and exploited.

---

\*Kindly correspond to [william.lugoloobi@oii.ox.ac.uk](mailto:william.lugoloobi@oii.ox.ac.uk)

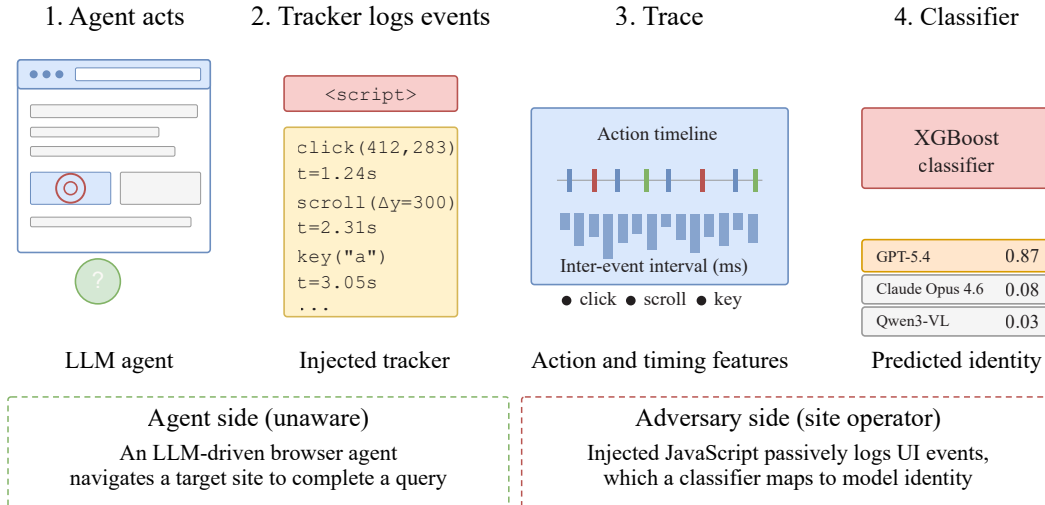


Figure 1: **Overview of our trace collection and threat model.** Using a JavaScript tracker, we collect actions performed by a browsing agent and train a classifier to predict model identity.

The main contributions of this paper are as follows:

- **Agent actions are a fingerprint of model identity.** We demonstrate for the first time that the on-page actions of LLM browser agents encodes the identity of the underlying model, achieving up to 96% classification Macro F1 across 14 frontier models using only behavioural traces collected via passive JavaScript injection.
- **A formalised threat model with defence analysis.** We characterise agent fingerprinting under a passive co-located adversary, and show that the attack is practical to maintain: new models can be enrolled by routing a small number of sessions through the instrumented site. We further show that standard browser normalisation with randomised delays is insufficient to remove the identifying signal when the adversary retrains their classifier on delayed traces.
- **Resources for agent fingerprinting.** We release a labelled corpus of agent interaction traces across four web environments and a browser harness compatible with both closed and open-source LLMs, enabling reproducible research into behavioural attribution of LLM agents.

## 2 Related Work

**LLM-based web agents.** Autonomous agents that combine language models with browser automation have rapidly moved from research prototypes to production systems [1–3]. Benchmarks such as WebArena [10] and Mind2Web [11] have established standard evaluation environments for these systems. As these agents are deployed at scale, the question of whether a site operator can determine which model is visiting becomes practically consequential for access control, content delivery, and adversarial exploitation.

**Bot detection and browser fingerprinting.** A large body of work studies how to distinguish automated from human web traffic. Early approaches relied on request-pattern heuristics and crawl detection [12–17]. Subsequent work has shown that fine-grained behavioural signals, such as mouse movements and interaction timing encode neuromotor structure that can reliably separate humans from bots [18, 19, 5, 20]. More recent systems combine behavioural features with server-side logs to detect increasingly sophisticated bots that mimic realistic browser fingerprints [4].

In parallel, browser fingerprinting research has demonstrated that passively collected client-side attributes (e.g., canvas, fonts, WebGL) can be combined into persistent identifiers at scale [6, 7]. Across these lines of work, the problem is typically framed as binary classification: human versus

bot. We instead consider a finer-grained setting: given that the user is an LLM-based agent, can we identify *which model* produced the interaction trace solely from its actions?

**Side-channel attacks and traffic fingerprinting.** Side-channel attacks show that systems leak sensitive information through correlated observables, even when their outputs do not [21]. Applied to web traffic, deep learning classifiers trained on encrypted packet sequences identify visited websites with over 98% accuracy [22, 23]. Cook et al. [24] draw a useful distinction between on-path attackers, who observe network traffic from a separate machine, and co-located attackers, whose code runs on the same machine as the victim. Our attack is co-located: we inject JavaScript trackers into the page and collect action traces directly, without any network-level visibility.

**LLM and agent fingerprinting.** Pasquini et al. [9] fingerprint LLM-integrated applications by sending crafted queries and analysing responses, achieving over 95% accuracy across 42 model versions. Beyond the result, they demonstrate that knowing the underlying model enables targeted attacks: an adversary who can identify the model can craft inputs that exploit model-specific behaviours, biases, or known failure modes, turning fingerprinting from a reconnaissance step [8, 25, 26] into an attack primitive. Closest to our setting, Zhang et al. [27] show that task-specific LLM agent applications leave distinct network traffic fingerprints. Their attack observes packet-level metadata generated by agent tool use, and uses it to infer behaviours, application identity, and downstream user attributes.

In contrast, we study model attribution from ordinary UI events generated while an agent browses a website. Because all agents in our experiments share the same browser harness and action space, our classifier targets the underlying model rather than a particular application, tool configuration, or interaction pattern. Our results thus show that the attribution surface extends beyond network observers and active probers to the visited page itself.

### 3 Problem Formulation

#### 3.1 Agent Identification as a Classification Problem

We study whether interaction traces produced by web-browsing agents contain sufficient signal to identify the underlying language model, and formalise this as a supervised classification problem over behavioural traces.

**Agent and environment.** An agent  $a \in \mathcal{A}$  is instantiated by a language model  $m \in \mathcal{M}$  interacting with a web environment  $\mathcal{E}$  through a fixed browser harness  $h$ . At each timestep  $t$ , the agent conditions on the current observation  $s_t$  (a rendered screenshot), updates an internal plan, and produces an action  $u_t$  (e.g., click, scroll, keypress). The environment executes  $u_t$ , yielding a new observation  $s_{t+1}$ , and the process repeats for  $N$  planning steps. We assume all agents share the same interface and action space, ensuring that any differences in behaviour arise from the underlying model rather than the execution environment.

**Interaction trace.** A session generates a trace

$$\tau = \{(s_t, u_t, \Delta t_t)\}_{t=1}^T,$$

where  $\Delta t_t$  denotes the time elapsed between consecutive actions. We restrict our analysis to client-side interaction signals, that is, the sequence and timing of actions produced by the agent, and do not use server-side metadata such as headers, IP addresses, or TLS fingerprints. Traces may span multiple pages within the same host and are treated as belonging to a single session tied to a query  $Q$ . We further restrict traces to a single domain to control for environmental variability.

**Identification task.** Given a trace  $\tau$  generated by an unknown agent, the goal is to predict the originating model

$$\hat{m} = f(\tau), \quad \hat{m} \in \mathcal{M},$$

where  $f$  is a classifier trained on labelled traces. Unlike prior work that frames this as human versus bot discrimination, we assume the client is automated and ask which model produced the behaviour.

**Feature creation.** We consider feature mappings  $\phi(\tau)$  derived from Inter-Event Intervals (IEIs, the time between two consecutive actions), navigation structure (e.g., click frequency and page

transitions), and interaction patterns (e.g., action type distributions). These features are designed to capture behavioural regularities induced by the underlying model. Full descriptions of extracted features are provided in Appendix A.5.

### 3.2 Threat Model

We consider a passive, co-located adversary: a site operator who injects pages with lightweight JavaScript to collect actions performed by an agent while visiting. Additionally, the adversary is assumed to have already established, via existing bot-detection methods, that the session originates from an automated agent rather than a human user [4]. Consequently, the identification problem becomes one of model attribution, not human-versus-bot detection.

The adversary has access to the sequence and timing of on-page actions, but no access to model internals, generated text, or network-layer traffic. We assume a realistic setting in which standard browser fingerprint signals are present alongside behavioural traces, and a fresh browser is instantiated for each session. The adversary is passive by assumption: they cannot modify page content or craft adversarial inputs to probe the agent directly. The adversary’s objective is identification: once the underlying model is known, they can consult a corpus of model-specific jailbreaks [28, 29] or initialise a targeted optimisation procedure [9, 30, 31] with a substantially reduced search space, bypassing the cost of generic black-box probing entirely.

Depending on the adversary’s knowledge of the agent population, this identification problem takes two forms.

**Closed-set fingerprinting.** Let  $\mathcal{A} = \{a_1, \dots, a_K\}$  be the full set of  $K$  agents. The adversary assumes that any observed trace originates from some  $a_i \in \mathcal{A}$  and learns a classifier  $f : \mathcal{T} \rightarrow \mathcal{A}$  over all  $K$  classes, where  $\mathcal{T}$  denotes the space of interaction traces  $\tau$ . At evaluation time, test traces are drawn from the same set  $\mathcal{A}$ , so the problem reduces to standard multi-class classification.

Notably a closed-set classifier can be **cheaply updated as new models are released**: the adversary need only route a small number of sessions through their instrumented site to enrol a new model into the classifier, without modifying the underlying collection infrastructure.

**Open-set fingerprinting.** In a more realistic setting, the adversary cannot know every agent they may encounter. Let  $\mathcal{A}_{\text{train}} \subset \mathcal{A}$  be the agents known at training time, and let  $\mathcal{A}_{\text{unk}} = \mathcal{A} \setminus \mathcal{A}_{\text{train}}$  denote the unknown agents. The classifier must either assign a trace to a known agent class or flag it as *unknown*.

We instantiate this setting via a **leave-one-agent-out (LOO)** protocol. Let  $K = |\mathcal{A}|$ . For each held-out agent  $a_i \in \mathcal{A}$ , we train a classifier on traces from  $\mathcal{A} \setminus \{a_i\}$  (all agents except  $a_i$ ) and evaluate on the test-split traces of the  $K - 1$  known agents together with all traces from  $a_i$  as the unknown class. We measure the ability to separate known from unknown traces using AUROC over the binary known/unknown discrimination, reported separately for each held-out agent  $a_i$ , yielding  $K$  values across the full agent set.

## 4 Experimental Setup

**Data** We construct a dataset spanning two broad task domains where agents have been widely applied: information seeking tasks and online shopping. For question answering, we repurpose 2WikiMultiHop [32] and FRAMES [33] as live web tasks, which requires models to navigate and retrieve information across multiple pages. Similarly, for shopping, we adapt the e-commerce benchmarks Webshop [34] and Deepshop [35]. Standard train, validation, and test splits for all datasets are summarised in Table 1. Together, these environments provide a broad basis for eliciting and comparing behavioural fingerprints across diverse interaction regimes. This structure also lets us distinguish in-domain attribution, cross-task transfer within a website, pooled site-level training, and cross-site transfer; we report these generalisation experiments in Appendix B.2.

**Models** We evaluate 14 multimodal LLMs selected to support model identity classification at two levels of granularity: model family (e.g., Qwen3-VL, Qwen3.5-VL) and specific model variant (e.g., Qwen3.5-9B vs. Qwen3.5-27B). Full details are given in Appendix A.1. Locally hosted open-source

Table 1: Dataset splits used in this work. All benchmarks are deployed as live web tasks on their respective target websites.

Dataset	Domain	Target Website	Train	Val	Test	Total
2WikiMultiHop [32]	QA	Wikipedia.com	150	75	75	300
FRAMES [33]	QA	Wikipedia.com	150	75	75	300
Webshop [34]	Shopping	Amazon.com	150	75	75	300
Deepshop [35]	Shopping	Amazon.com	75	37	38	150
<b>Total</b>			525	262	263	1050

models span four families: the GLM-4.6V [36], Qwen3-VL series [37], Qwen3.5-VL series [38], UI-TARS-1.5-7B [39] (a UI-specialist fine-tune of Qwen2.5-VL [40]), and the Gemma-4 series [41]. We additionally include Seed-2.0-Lite [42], an open-weight model accessed via OpenRouter. Proprietary frontier models, namely GPT-5.4 [43], Gemini-3.1 and Gemini-3-Flash [44], and Claude Opus 4.6 [45], are evaluated via their respective APIs.

**Agent Harness** We standardise our computer-use harness with Midscene.js [46], a JavaScript library that provides a standardised interface between multimodal LLMs and browser environments, enabling models to perceive and interact with web-based UIs by translating actions into Playwright commands. All agents share an identical harness configuration, ensuring that behavioural differences between traces are attributable to the underlying model rather than the harness. Since Midscene.js operates in pure-vision mode only, browser observations are limited to visual screenshots; this also suits our setting, as it ensures any identifying signal derives from visual reasoning and interaction behaviour rather than from differences in how models process structured markup.

**Trace collection** We instrument each page with a lightweight JavaScript observer injected at session initialisation. The observer attaches event listeners to the DOM and records every interaction event produced by the agent, including click coordinates and target element type, scroll direction and magnitude, keypress events and inter-keystroke timing, and navigation events with timestamps. All events are logged with millisecond-resolution timestamps relative to session start, yielding a raw event stream that is post-processed into the structured trace format  $\tau = \{(s_t, u_t, \Delta t_t)\}_{t=1}^T$  defined in Section 3. A fresh browser context is instantiated for each session to prevent cross-session state leakage. Each agent completes every query in the dataset independently, yielding a labelled corpus of traces with model identity as the class label.

**Classifiers** We train five classifier families on the collected traces: Lasso Regression, Logistic Regression, Random Forest, XGBoost, and an LSTM network. We report results primarily for XGBoost, which achieves the strongest performance across datasets; full results for all classifiers are provided in Appendix A.3.

**Metrics** To evaluate our classifiers in the closed-set fingerprinting setting, we report the per-LLM F1 score and the macro F1 across all classifiers. For the open-set fingerprinting setting, we report the AUROC for each classifier.

**Hardware** All Open-Source Models are served via vLLM on a node equipped with two NVIDIA H100 GPUs.

## 5 Fingerprinting Results

### 5.1 Agents are identifiable from traces of their actions

**Known LLMs are broadly fingerprintable from their actions.** In the closed-set setting, agents are highly identifiable from action traces. Across all four benchmarks in Figure 2, our XGBoost classifier recovers the source model at roughly  $10\times$  random chance, with per-agent F1 exceeding 70% for the majority of models on every dataset. Top performers such as Seed-2-lite (96.1% on 2WikiMultiHopQA) and UI-TARS-1.5 (92.1% on WebShop) are near-perfectly identifiable,

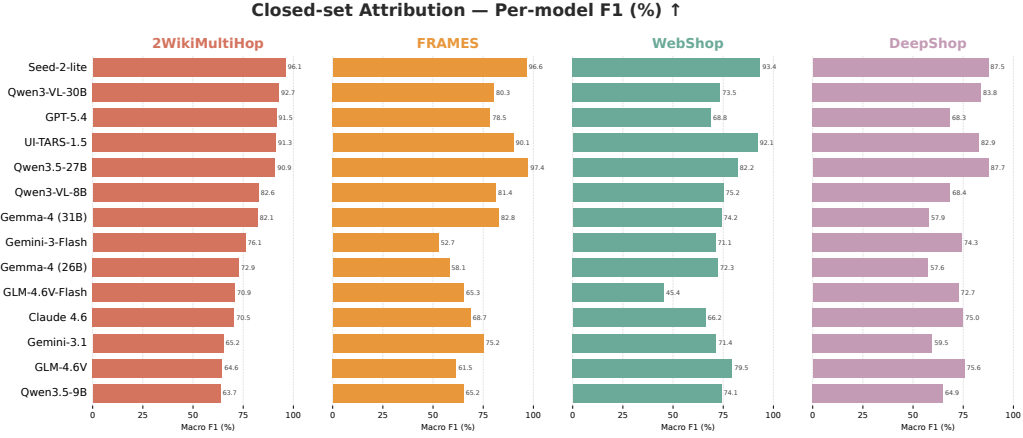


Figure 2: **Agents are identifiable from traces of their actions.** Across both information-seeking and shopping benchmarks, our XGBoost classifier trained on action traces reliably identifies the browsing agent. High scores across all four datasets indicate that agents leave consistent, distinctive traces in their browsing actions.

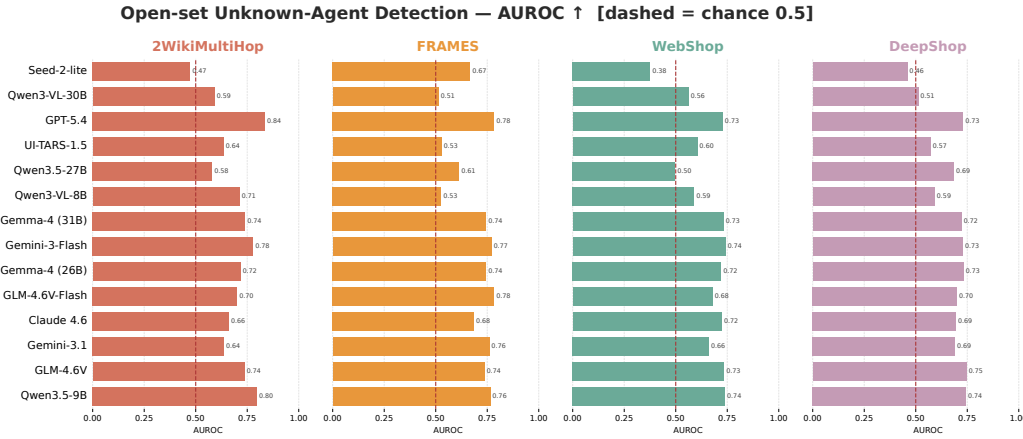


Figure 3: **Unknown agents are detectable above chance, but identification remains an open challenge.** Detection is consistently above chance across all four datasets, with the majority of agents exceeding AUROC 0.60 with our XGBoost classifier. A notable exception is Seed-2-lite, which scores below chance on 2WikiMultiHopQA, WebShop, and DeepShop despite achieving the highest closed-set identifiability. Nevertheless, robust open-set identification remains an open challenge.

suggesting their actions are highly consistent and distinct across episodes. Performance remains high even on the weakest pair (63.7% for Qwen3.5-9B on 2WikiMultiHopQA), well above the ~7% random baseline for 14 classes. This extends to family-level attribution: grouping agents by model family preserves strong identifiability without version-specific labels (Appendix 11). We explore generalisation across tasks and sites in Appendix B.2, finding that single-task transfer is weak but pooling traces from multiple tasks on the same site recovers strong attribution.

**Open-set fingerprinting is agent-specific and orthogonal to closed-set performance.** Detection of unknown models is consistently above chance across all four datasets and most agents, with the majority exceeding  $AUROC \approx 0.60$ . However, agents that are easiest to classify when their identities are known (closed-set) are not easy to classify in an open-set setting. Most strikingly, Seed-2-lite (the best-identified agent in the closed-set setting) scores below chance on three of four datasets (AUROC 0.47 on 2WikiMultiHopQA, 0.38 on WebShop, 0.46 on DeepShop), while GPT-5.4 achieves the highest open-set AUROC overall (0.84 on 2WikiMultiHopQA) despite ranking third in closed-set F1.

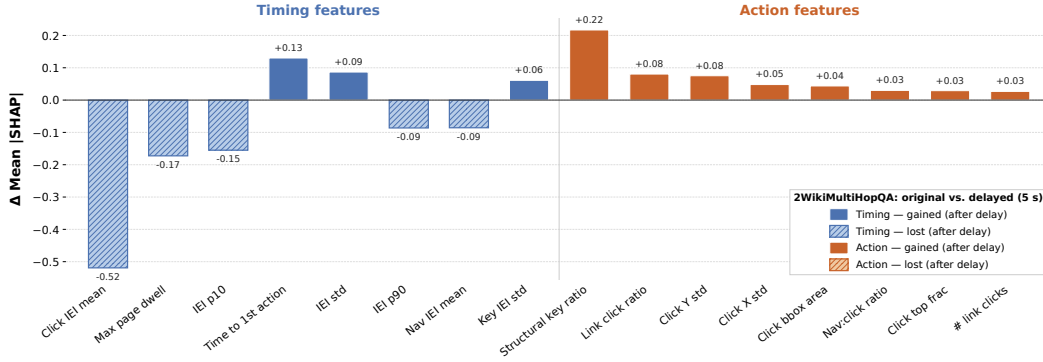


Figure 4: **Timing features are important but sensitive to perturbation, while action features are robust.** Each bar shows the change in mean |SHAP| for a feature when XGBoost is retrained on 5-second-delayed traces. Under normal conditions, timing features based on IEI statistics and time to first action dominate agent identification, but after training on delayed traces, our classifier relies on action-centred features like structural key ratio and click position to make predictions.

This dissociation suggests that closed-set identifiability reflects how distinct an agent is within a known distribution, whilst open-set identifiability punishes models whose behaviour isn’t uniquely distinct from that of known agents.

In general, this demonstrates that open-set detection is useful even when exact attribution is impossible: for a website host, recognising that a visiting trace belongs to no currently enrolled model is sufficient to trigger offline collection and later enrollment into the fingerprint database.

## 6 Analysis

### 6.1 Timing dominates the fingerprint, but actions are more robust to perturbation

**Timing is the primary signal.** We compute mean absolute SHAP values for the XGBoost classifier on 2WikiMultiHopQA before and after retraining on delayed traces in Figure 4. *Initially*, our top features, are overwhelmingly timing-based: IEI standard deviation, mean click IEI, and time to first action all receive substantially larger attributions than structural features like key ratio. Agents are distinguishable not primarily by what actions they take, but by their tempo: how long they pause before acting, how variable that pause is, and whether different action types carry their own characteristic delays. Full feature SHAP results are presented in Appendix B.3. Aside from these features, we show that classifier performance isn’t tied to overall agent capability in Appendix B.1.

**Actions carry the fingerprint when timing is disrupted.** If classifiers rely on temporal signatures, adding random delays should be enough to break them. We test this by injecting a uniformly sampled random delay between agent actions at test time and evaluating XGBoost under increasing delay budgets in Figure 5. Without retraining, macro F1 drops sharply as injected delay grows, confirming that clean-trace classifiers are sensitive to disrupted timing rhythms. However, retraining on delayed traces largely recovers performance across all four datasets. The classifier shifts weight onto features that survive delay injection: residual timing variability, click-coordinate dispersion, structural key ratio, and link-click ratio. These are features grounded in **what** agents do and, not merely **when**.

### 6.2 Agent fingerprinting is efficient at both training and test time

**Strong classifiers can be trained from few observed events.** By varying the proportion of training data used to fit our XGBoost classifier, we find that fewer than one third of traces are sufficient to approach peak classification performance across all four datasets (Figure 6A). Gains diminish rapidly beyond this point, indicating that the behavioural signatures underpinning agent identity are both consistent and learnable from modest supervision.

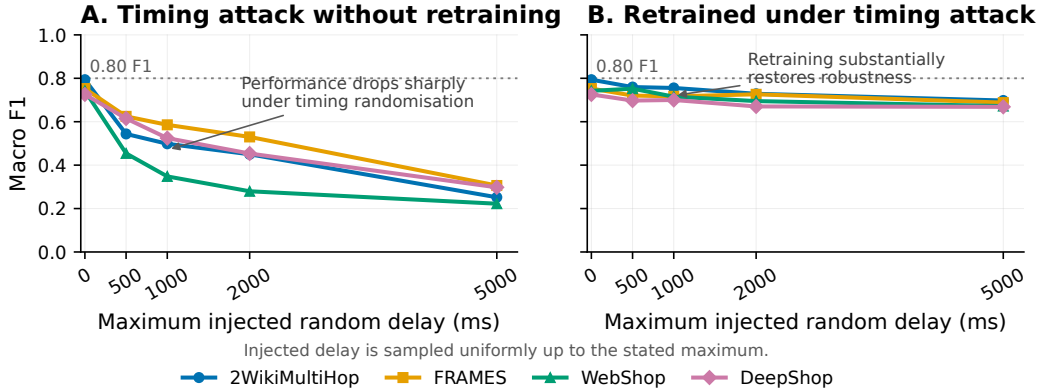


Figure 5: **Simple timing delays weaken unadapted classifiers but not adaptive ones.** (Left) Performance of an unadapted classifier, trained on clean traces and evaluated under increasing injected delays. (Right) Performance of a delay-adapted classifier, retrained on delayed traces and evaluated under the same perturbation. While delay injection substantially degrades the unadapted classifier, performance largely recovers after retraining.

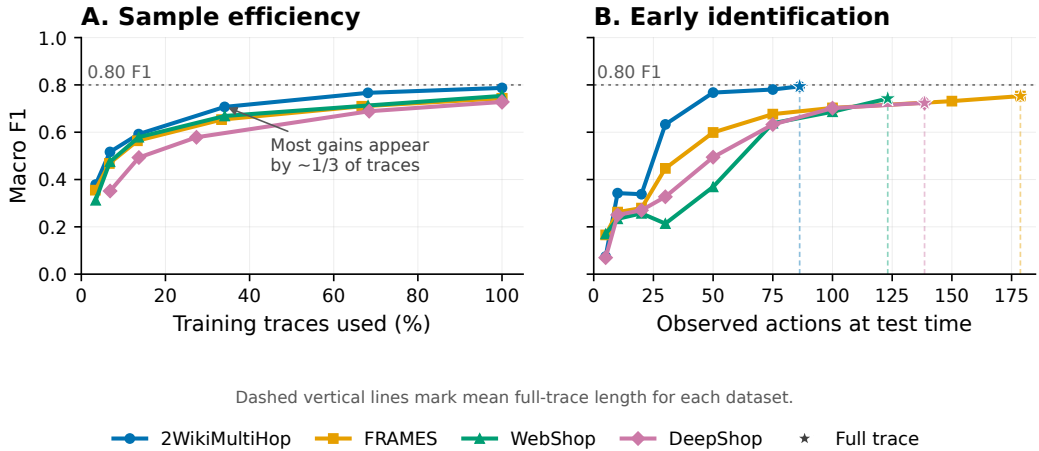


Figure 6: **Agent fingerprints emerge early and can be learned from short traces.** (Left) Training efficiency, measured by training classifiers using only the first  $k$  events from each training trace and evaluating them on full held-out traces. (Right) Identification speed, measured by training classifiers on full traces and evaluating them using only the first  $k$  events observed at test time. Dashed vertical lines mark the mean full-trace length for each dataset.

**Agent identity can be inferred early at test time.** Using our XGBoost classifier trained on full traces, we systematically reduce the number of events observed at test time to assess how quickly identity can be recovered mid-trajectory. As shown in Figure 6B, macro F1 rises sharply within the first 40% of observed actions across all datasets, after which performance plateaus near that of the full-trace classifier. This means a site operator does not need to wait for a session to complete before attributing its model: identification can occur while the agent is still navigating the page, leaving ample opportunity to condition a subsequent attack on the inferred identity.

## 7 Implications

### 7.1 Attack Surface: Agent-Targeted Exploits

Knowing the identity of a target makes an adversary’s job easier, reducing the search space from all possible attacks to those known to be effective against the target [8]. A natural application is the class

of threats known as AI Agent Traps: adversarial page content designed to manipulate, deceive, or exploit visiting agents [47]. Passive fingerprinting lets each trap be conditioned on model identity, converting generic exploits into targeted ones across three attack surfaces we characterise below

**Model-specific prompt injection.** LLMs exhibit systematically different susceptibilities to prompt injection [30, 9]. Without identity information, an adversary must either deploy generic injections that may be ineffective, or mount a costly black-box search over model-specific failure modes, both of which are detectable and expensive. Action fingerprinting collapses this search *passively*: once the model is identified, the adversary can select directly from a known corpus of model-specific jailbreaks [29, 28] or initialise a targeted optimisation with a substantially reduced search space [30, 9, 31]. Because fingerprinting is passive and robust to timing delays, a visiting agent has no signal that it is being identified. Furthermore, since the injection payload can be conditioned on the inferred identity after fingerprinting completes, it is invisible to any visitor whose model does not match the target, making such attacks difficult to detect through conventional crawling or auditing.

**Adversarial cost inflation.** Sponge attacks aim to exhaust the computational budget of neural networks by inducing verbose or high-entropy reasoning [48]. Agent identifiability introduces a targeted variant: a site operator who knows which model is visiting can serve that model pages calibrated to maximise its token consumption, through navigational ambiguity, redundant content, or structures known to trigger extended reasoning, while serving normal content to all other visitors. This constitutes a denial-of-service vector targeting the *user's* inference budget rather than the host's compute, a threat class that to our knowledge has not been previously formalised. It is particularly consequential for high-cost frontier models such as Claude Opus 4.6 or GPT-5.4, where modest per-query cost increases compound significantly at scale.

**Agent-specific access control.** Beyond active exploitation, identity signals let site operators route content by model identity. We anticipate two near-term variants. *Blacklisting* denies service to specific models for cost, legal, or competitive reasons without blocking agents broadly. *Whitelisting*, the more adversarial inverse, serves model-conditioned content that misleads specific agents while appearing benign to others. This is especially dangerous because poisoned content may be invisible to auditors using a different model. Neither variant requires a fixed classifier: a site operator can *continuously retrain* on organic or simulated traces, extending coverage to new models without external data. Appendix B.2 supports this assumption: although single-task transfer is weak, pooling multiple tasks from the same website recovers strong attribution.

## 8 Conclusion

We show that UI actions from agent traces can fingerprint the underlying model of an LLM-based web agent with up to 96% F1 across 14 frontier models. The signal is typically recoverable from fewer than 15 observed events and does not rely on browser attributes, network-layer visibility, or active probing.

The practical consequence is a shift in the threat landscape for deployed agents. Target identification is the first step towards exploitation, and we show that this move can be executed passively during ordinary navigation by any party that controls a page visited by the agent. Every page visit thus becomes a potential attribution event on which model-specific injections, content poisoning, or budget exhaustion can be conditioned.

The operative question for the next generation of agent-aware web infrastructure is therefore no longer whether a client is human or automated, but which model is producing the behaviour. Within-agent attribution, rather than bot detection, is the axis on which both defences and cooperative protocols should be designed. We release our trace corpus and evaluation harness to make that axis measurable.

Our study is only the first step towards full identification: we use a single agent harness (Midscene.js), a closed set of 14 frontier models, and open-set detection that remains imperfect. Future work should characterise harness-invariant signals, evaluate obfuscation defences against adaptive adversaries, and extend classification to agents that flexibly browse through either HTML parsing or visual GUI reasoning.

Overall, as LLM-based agents become a standard client of the web, their on-page behaviour is an identifying signal that warrants the same engineering scrutiny as the models themselves. Attackers and operators now have access to the same primitive, and the design of agent-aware infrastructure will be shaped by how each chooses to use it. Whether it is used to exploit agents or to serve them better, the primitive is now available to both.

## 9 Acknowledgements

LW and JM were supported by a Rhodes Scholarship. SM was supported by the EPSRC Centre for Doctoral Training in Autonomous Intelligent Machines and Systems n. EP/Y035070/1, in addition to Microsoft Ltd.

## References

- [1] Reiichiro Nakano, Jacob Hilton, Suchir Balaji, Jeff Wu, Long Ouyang, Christina Kim, Christopher Hesse, Shantanu Jain, Vineet Kosaraju, William Saunders, Xu Jiang, Karl Cobbe, Tyna Eloundou, Gretchen Krueger, Kevin Button, Matthew Knight, Benjamin Chess, and John Schulman. WebGPT: Browser-assisted question-answering with human feedback, June 2022. URL <http://arxiv.org/abs/2112.09332>. arXiv:2112.09332.
- [2] Shunyu Yao, Jeffrey Zhao, Dian Yu, Nan Du, Izhak Shafran, Karthik R. Narasimhan, and Yuan Cao. ReAct: Synergizing Reasoning and Acting in Language Models. September 2022. URL [https://openreview.net/forum?id=wE\\_vluYUL-X](https://openreview.net/forum?id=wE_vluYUL-X).
- [3] Lei Wang, Chen Ma, Xueyang Feng, Zeyu Zhang, Hao Yang, Jingsen Zhang, Zhiyuan Chen, Jiakai Tang, Xu Chen, Yankai Lin, Wayne Xin Zhao, Zhewei Wei, and Jirong Wen. A survey on large language model based autonomous agents. *Frontiers of Computer Science*, 18(6): 186345, March 2024. ISSN 2095-2236. doi: 10.1007/s11704-024-40231-1. URL <https://doi.org/10.1007/s11704-024-40231-1>.
- [4] Christos Iliou, Theodoros Kostoulas, Theodora Tsikrika, Vasilios Katos, Stefanos Vrochidis, and Ioannis Kompatsiaris. Detection of Advanced Web Bots by Combining Web Logs with Mouse Behavioural Biometrics. In *Digital Threats: Research and Practice*, volume 2, 2021. URL <https://dl.acm.org/doi/10.1145/3447815>.
- [5] Alejandro Acien, Aythami Morales, Julian Fierrez, and Ruben Vera-Rodriguez. BeCAPTCHA-Mouse: Synthetic Mouse Trajectories and Improved Bot Detection. *Pattern Recognition*, 127: 108643, 2022. URL <https://arxiv.org/abs/2005.00890>.
- [6] Peter Eckersley. How Unique Is Your Web Browser? In *Privacy Enhancing Technologies Symposium (PETS)*, pages 1–18. Springer, 2010. URL <https://panopticclick.eff.org/static/browser-uniqueness.pdf>.
- [7] Antoine Vastel, Pierre Laperdrix, Walter Rudametkin, and Romain Rouvoy. FP-Stalker: Tracking Browser Fingerprint Evolutions. In *IEEE Symposium on Security and Privacy*, pages 728–741, 2018. URL <https://arxiv.org/abs/1805.09046>.
- [8] Eric M. Hutchins, Michael J. Cloppert, and Rohan M. Amin. Intelligence-Driven Computer Network Defense Informed by Analysis of Adversary Campaigns and Intrusion Kill Chains. Technical report, Lockheed Martin Corporation, 2011. URL <https://lockheedmartin.com/content/dam/lockheed-martin/rms/documents/cyber/LM-White-Paper-Intel-Driven-Defense.pdf>.
- [9] Dario Pasquini, Evgenios M. Kornaropoulos, and Giuseppe Ateniese. LLMmap: Fingerprinting for Large Language Models. pages 299–318, 2025. ISBN 978-1-939133-52-6. URL <https://www.usenix.org/conference/usenixsecurity25/presentation/pasquini>.
- [10] Shuyan Zhou, Frank F Xu, Hao Zhu, Xuhui Zhou, Robert Lo, Abishek Sridhar, Xianyi Cheng, Yonatan Bisk, Daniel Fried, Uri Alon, and others. WebArena: A Realistic Web Environment for Building Autonomous Agents. *arXiv preprint arXiv:2307.13854*, 2023.

- [11] Xiang Deng, Yu Gu, Boyuan Zheng, Shijie Chen, Samuel Stevens, Boshi Wang, Huan Sun, and Yu Su. Mind2Web: Towards a Generalist Agent for the Web, 2023. [\\_eprint: 2306.06070](#).
- [12] T. Kabe and M. Miyazaki. Determining WWW user agents from server access log. In *Proceedings Seventh International Conference on Parallel and Distributed Systems: Workshops*, pages 173–178, 2000. doi: 10.1109/PADSW.2000.884534.
- [13] Paul Huntington, David Nicholas, and Hamid R. Jamali. Web robot detection in the scholarly information environment. *J. Inf. Sci.*, 34(5):726–741, October 2008. ISSN 0165-5515. doi: 10.1177/0165551507087237. URL <https://doi.org/10.1177/0165551507087237>.
- [14] Nick Geens, Johan Huysmans, and Jan Vanthienen. Evaluation of Web Robot Discovery Techniques: A Benchmarking Study. In Petra Perner, editor, *Advances in Data Mining. Applications in Medicine, Web Mining, Marketing, Image and Signal Mining*, pages 121–130, Berlin, Heidelberg, 2006. Springer. ISBN 978-3-540-36037-7. doi: 10.1007/11790853\_10.
- [15] Martijn Koster. The Web Robots Pages, 1994. URL <https://www.robotstxt.org/orig.html>.
- [16] Martijn Koster, Gary Illyes, Henner Zeller, and Lizzi Sassman. Robots Exclusion Protocol. Request for Comments RFC 9309, Internet Engineering Task Force, September 2022. URL <https://datatracker.ietf.org/doc/rfc9309>. Num Pages: 12.
- [17] Derek Doran and Swapna S. Gokhale. Web robot detection techniques: overview and limitations. *Data Mining and Knowledge Discovery*, 22(1):183–210, January 2011. ISSN 1573-756X. doi: 10.1007/s10618-010-0180-z. URL <https://doi.org/10.1007/s10618-010-0180-z>.
- [18] Shen Fu, Dong Qin, Daji Qiao, and George T Amariuca. RUMBA-Mouse: Rapid User Mouse-Behavior Authentication Using a CNN-RNN Approach. In *2020 IEEE Conference on Communications and Network Security (CNS)*, pages 1–9. IEEE, 2020. ISBN 978-1-7281-4760-4.
- [19] Yi Wang, Chengyv Wu, Yang Liao, and Maowei You. Optimizing Mouse Dynamics for User Authentication by Machine Learning: Addressing Data Sufficiency, Accuracy-Practicality Trade-off, and Model Performance Challenges, May 2025. URL <http://arxiv.org/abs/2504.21415>. arXiv:2504.21415 [cs].
- [20] Penny Chong, View Profile, Yuval Elovici, View Profile, Alexander Binder, and View Profile. User Authentication Based on Mouse Dynamics Using Deep Neural Networks: A Comprehensive Study. *IEEE Transactions on Information Forensics and Security*, 15:1086–1101, January 2020. doi: 10.1109/TIFS.2019.2930429. URL <https://dl.acm.org/doi/abs/10.1109/TIFS.2019.2930429>.
- [21] Paul C. Kocher. Timing Attacks on Implementations of Diffie-Hellman, RSA, DSS, and Other Systems. In *Advances in Cryptology (CRYPTO)*, pages 104–113. Springer, 1996. URL <https://www.paulkocher.com/doc/TimingAttacks.pdf>.
- [22] Vera Rimmer, Davy Preuveneers, Marc Juarez, Tom Van Goethem, and Wouter Joosen. Automated Website Fingerprinting through Deep Learning. In *Network and Distributed System Security Symposium (NDSS)*, 2018. URL <https://arxiv.org/abs/1708.06376>.
- [23] Payap Sirinam, Mohsen Imani, Marc Juarez, and Matthew Wright. Deep Fingerprinting: Undermining Website Fingerprinting Defenses with Deep Learning. In *ACM Conference on Computer and Communications Security (CCS)*, pages 1928–1943, 2018. URL <https://arxiv.org/abs/1801.02265>.
- [24] Jack Cook, Jules Drean, Jonathan Behrens, and Mengjia Yan. There’s always a bigger fish: a clarifying analysis of a machine-learning-assisted side-channel attack. In *Proceedings of the 49th Annual International Symposium on Computer Architecture, ISCA ’22*, pages 204–217, New York, NY, USA, June 2022. Association for Computing Machinery. ISBN 978-1-4503-8610-4. doi: 10.1145/3470496.3527416. URL <https://dl.acm.org/doi/10.1145/3470496.3527416>.

- [25] MITRE Corporation. MITRE ATT&CK: Adversarial Tactics, Techniques and Common Knowledge, 2025. URL <https://attack.mitre.org>.
- [26] Shaked Zychlinski. A Whole New World: Creating a Parallel-Poisoned Web Only AI-Agents Can See, August 2025. URL <http://arxiv.org/abs/2509.00124>. arXiv:2509.00124 [cs] version: 1.
- [27] Yixiang Zhang, Xinhao Deng, Zhongyi Gu, Yihao Chen, Ke Xu, Qi Li, and Jianping Wu. Exposing LLM User Privacy via Traffic Fingerprint Analysis: A Study of Privacy Risks in LLM Agent Interactions, October 2025. URL <http://arxiv.org/abs/2510.07176>. arXiv:2510.07176 [cs] version: 1.
- [28] Andy Zou, Zifan Wang, Nicholas Carlini, Milad Nasr, J. Zico Kolter, and Matt Fredrikson. Universal and Transferable Adversarial Attacks on Aligned Language Models, December 2023. URL <http://arxiv.org/abs/2307.15043>. arXiv:2307.15043 [cs].
- [29] Xinyue Shen, Zeyuan Chen, Michael Backes, Yun Shen, and Yang Zhang. “Do Anything Now”: Characterizing and Evaluating In-The-Wild Jailbreak Prompts on Large Language Models. *arXiv preprint arXiv:2308.03825*, 2024.
- [30] Lukas Aichberger, Alasdair Paren, Yarin Gal, Philip Torr, and Adel Bibi. Attacking Multimodal OS Agents with Malicious Image Patches, March 2025. URL <http://arxiv.org/abs/2503.10809>. arXiv:2503.10809 [cs].
- [31] Dominik Seip and Matthias Hein. Preference Redirection via Attention Concentration: An Attack on Computer Use Agents, April 2026. URL <http://arxiv.org/abs/2604.08005>. arXiv:2604.08005 [cs].
- [32] Xanh Ho, Anh-Khoa Duong Nguyen, Saku Sugawara, and Akiko Aizawa. Constructing A Multi-hop QA Dataset for Comprehensive Evaluation of Reasoning Steps. In Donia Scott, Nuria Bel, and Chengqing Zong, editors, *Proceedings of the 28th International Conference on Computational Linguistics*, pages 6609–6625, Barcelona, Spain (Online), December 2020. International Committee on Computational Linguistics. doi: 10.18653/v1/2020.coling-main.580. URL <https://aclanthology.org/2020.coling-main.580/>.
- [33] Satyapriya Krishna, Kalpesh Krishna, Anhad Mohananeey, Steven Schwarcz, Adam Stambler, Shyam Upadhyay, and Manaal Faruqui. Fact, Fetch, and Reason: A Unified Evaluation of Retrieval-Augmented Generation, January 2025. URL <http://arxiv.org/abs/2409.12941>. arXiv:2409.12941 [cs].
- [34] Shunyu Yao, Howard Chen, John Yang, and Karthik Narasimhan. WebShop: Towards Scalable Real-World Web Interaction with Grounded Language Agents, February 2023. URL <http://arxiv.org/abs/2207.01206>. arXiv:2207.01206 [cs].
- [35] Yougang Lyu, Xiaoyu Zhang, Lingyong Yan, Maarten de Rijke, Zhaochun Ren, and Xiuying Chen. DeepShop: A Benchmark for Deep Research Shopping Agents, June 2025. URL <http://arxiv.org/abs/2506.02839>. arXiv:2506.02839 [cs].
- [36] V. Team, Wenyi Hong, Wenmeng Yu, Xiaotao Gu, Guo Wang, Guobing Gan, Haomiao Tang, Jiale Cheng, Ji Qi, Junhui Ji, Lihang Pan, Shuaiqi Duan, Weihang Wang, Yan Wang, Yean Cheng, Zehai He, Zhe Su, Zhen Yang, Ziyang Pan, Aohan Zeng, Baoxu Wang, Bin Chen, Boyan Shi, Changyu Pang, Chenhui Zhang, Da Yin, Fan Yang, Guoqing Chen, Jiazheng Xu, Jiale Zhu, Jiali Chen, Jing Chen, Jinhao Chen, Jinghao Lin, Jinjiang Wang, Junjie Chen, Leqi Lei, Letian Gong, Leyi Pan, Mingdao Liu, Mingde Xu, Mingzhi Zhang, Qinkai Zheng, Sheng Yang, Shi Zhong, Shiyu Huang, Shuyuan Zhao, Siyan Xue, Shangqin Tu, Shengbiao Meng, Tianshu Zhang, Tianwei Luo, Tianxiang Hao, Tianyu Tong, Wenkai Li, Wei Jia, Xiao Liu, Xiaohan Zhang, Xin Lyu, Xinyue Fan, Xuancheng Huang, Yanling Wang, Yadong Xue, Yanfeng Wang, Yanzi Wang, Yifan An, Yifan Du, Yiming Shi, Yiheng Huang, Yilin Niu, Yuan Wang, Yuanchang Yue, Yuchen Li, Yutao Zhang, Yuting Wang, Yu Wang, Yuxuan Zhang, Zhao Xue, Zhenyu Hou, Zhengxiao Du, Zihan Wang, Peng Zhang, Debing Liu, Bin Xu, Juanzi Li, Minlie Huang, Yuxiao Dong, and Jie Tang. GLM-4.5V and GLM-4.1V-Thinking: Towards Versatile Multimodal Reasoning with Scalable Reinforcement Learning, 2025. URL <https://arxiv.org/abs/2507.01006>. \_eprint: 2507.01006.

- [37] Qwen Team. Qwen3 Technical Report, 2025. URL <https://arxiv.org/abs/2505.09388>.  
\_eprint: 2505.09388.
- [38] Qwen Team. Qwen3.5: Towards Native Multimodal Agents, February 2026. URL <https://qwen.ai/blog?id=qwen3.5>.
- [39] Yujia Qin, Yining Ye, Junjie Fang, Haoming Wang, Shihao Liang, Shizuo Tian, Junda Zhang, Jiahao Li, Yunxin Li, Shijue Huang, Wanjun Zhong, Kuanye Li, Jiale Yang, Yu Miao, Woyu Lin, Longxiang Liu, Xu Jiang, Qianli Ma, Jingyu Li, Xiaojun Xiao, Kai Cai, Chuang Li, Yaowei Zheng, Chaolin Jin, Chen Li, Xiao Zhou, Minchao Wang, Haoli Chen, Zhaojian Li, Haihua Yang, Haifeng Liu, Feng Lin, Tao Peng, Xin Liu, and Guang Shi. UI-TARS: Pioneering Automated GUI Interaction with Native Agents, January 2025. URL <http://arxiv.org/abs/2501.12326>. arXiv:2501.12326 [cs].
- [40] Shuai Bai, Keqin Chen, Xuejing Liu, Jialin Wang, Wenbin Ge, Sibao Song, Kai Dang, Peng Wang, Shijie Wang, Jun Tang, Humen Zhong, Yuanzhi Zhu, Mingkun Yang, Zhaohai Li, Jianqiang Wan, Pengfei Wang, Wei Ding, Zheren Fu, Yiheng Xu, Jiabo Ye, Xi Zhang, Tianbao Xie, Zesen Cheng, Hang Zhang, Zhibo Yang, Haiyang Xu, and Junyang Lin. Qwen2.5-VL Technical Report. *arXiv preprint arXiv:2502.13923*, 2025.
- [41] Gemma Team. Gemma 4, 2026. URL <https://deepmind.google/models/gemma/gemma-4/>.
- [42] ByteDance Seed Team. Seed2.0 Model Card, 2026. URL <https://github.com/ByteDance-Seed/Seed2.0>.
- [43] OpenAI. Introducing GPT-5.4, April 2026. URL <https://openai.com/index/introducing-gpt-5-4/>.
- [44] Google. Gemini 3.1 Pro. URL <https://deepmind.google/models/gemini/pro/>.
- [45] Anthropic. Claude Opus 4.6. URL <https://www.anthropic.com/news/claude-opus-4-6>.
- [46] YiBing Lin Xiao Zhou, Tao Yu. Midscene.js: Your AI Operator for Web, Android, iOS, Automation & Testing., 2025. URL <https://github.com/web-infra-dev/midscene>.
- [47] Matija Franklin, Nenad Tomašev, Julian Jacobs, Joel Z. Leibo, and Simon Osindero. AI Agent Traps, March 2026. URL <https://papers.ssrn.com/abstract=6372438>.
- [48] Iliia Shumailov, Yiren Zhao, Daniel Bates, Nicolas Papernot, Robert Mullins, and Ross Anderson. Sponge Examples: Energy-Latency Attacks on Neural Networks. In *2021 IEEE European Symposium on Security and Privacy (EuroS&P)*, pages 212–231, September 2021. doi: 10.1109/EuroSP51992.2021.00024. URL <https://ieeexplore.ieee.org/document/9581273>.

## Appendix

### A Additional Experimental Details

#### A.1 LLMs Used

Table 2: Models evaluated in this work. <sup>‡</sup>UI-specialist model fine-tuned for GUI agent tasks. Active parameter counts shown for mixture-of-experts (MoE) models.

Model	Type	Params	Active	Access
<i>Open-source — locally hosted</i>				
Qwen3-VL-8B [37]	General	8B	8B	Local
Qwen3-VL-30B-A3B [37]	General	30B	3B	Local
Qwen3.5-9B [38]	General	9B	9B	Local
Qwen3.5-27B [38]	General	27B	27B	Local
GLM-4.6V [36]	General	106B	—	Local
GLM-4.6V-Flash [36]	General	9B	—	Local
UI-TARS-1.5-7B <sup>‡</sup> [39]	UI-specialist	7B	7B	Local
Gemma-4-26B-A4B [41]	General	26B	4B	Local
Gemma-4-31B [41]	General	31B	31B	Local
<i>Proprietary — API</i>				
GPT-5.4 [43]	General	—	—	API
Gemini-3.1 [44]	General	—	—	API
Gemini-3-Flash [44]	General	—	—	API
Claude Opus 4.6 [45]	General	—	—	API
Seed-2.0-Lite [42]	General	—	—	API

#### A.2 Prompt Templates for Datasets

**Task: Wikipedia Question Answering**

You are browsing Wikipedia to answer a question.

**Rules:**

- Restrict browsing to <https://www.wikipedia.org>.
- Use the browser to gather evidence before answering.
- Output the final answer as `<answer>...</answer>`.

**Question:**

{question}

**Task: Amazon Product Selection**

You are a shopping assistant tasked with finding the product that best matches the description.

**Instructions:**

- Browse Amazon freely (search, filter, and view product pages).
- Add promising items to your cart and refine your selection.
- Remove items if better alternatives are found.
- Do not log in or proceed to checkout.

At completion, your cart should contain only the product(s) that best match the description.

**Description:**

{description}

### A.3 Classifier Hyperparameters

We train four classifier families on the behavioural feature set described in Section A.5: a Random Forest, XGBoost, two Logistic Regression variants (L2 and L1), and a hybrid LSTM. All classifiers are selected by validation accuracy via cross-validated hyperparameter search; final models are refit on the training split only.

**Random Forest.** Exhaustive grid search (3-fold CV) over the space in Table 3. Features are used without scaling.

Hyperparameter	Search space
n_estimators	200, 400
max_depth	None (unlimited), 15, 30
max_features	sqrt, log2, 0.4
min_samples_split	2, 5

Table 3: Random Forest hyperparameter grid (exhaustive,  $2 \times 3 \times 3 \times 2 = 36$  configurations).

**XGBoost.** Randomised search (40 iterations, 3-fold CV, hist tree method) over the space in Table 4. Features are used without scaling.

Hyperparameter	Search space
n_estimators	100, 200, 300, 400, 500
learning_rate	0.01, 0.05, 0.1, 0.2, 0.3
max_depth	3, 4, 5, 6, 7, 8
subsample	0.6, 0.7, 0.8, 0.9, 1.0
colsample_bytree	0.5, 0.6, 0.7, 0.8, 1.0
reg_alpha	0, 0.01, 0.1, 1.0
reg_lambda	0.5, 1.0, 2.0, 5.0

Table 4: XGBoost hyperparameter search space (randomised, 40 draws).

**Logistic Regression.** We train two variants with 3-fold grid search over  $C \in \{0.01, 0.1, 1.0, 10.0\}$ , with a maximum of 5,000 iterations. Features are  $z$ -score normalised (StandardScaler fit on training data only). LR-L2 uses the lbfgs solver; LR-Lasso uses the saga solver with full L1 regularisation.

**LSTM.** The AgentLSTM encodes the raw browser event sequence. Each event is represented as a token embedding (dimension 16) concatenated with five continuous scalars: log inter-event gap, log absolute session timestamp, spatial position (normalised click  $x/y$  or scroll depth), and log running per-type inter-event interval. The token vocabulary covers eight event types (click, keydown, scroll, navigate, beforeunload, focus, plus <pad> and <unk>). The LSTM final hidden state is concatenated with the pre-computed aggregate feature vector before the classification head.

Fixed training hyperparameters are listed in Table 5; the grid searched over hidden dimension and dropout is given in Table 6. Best configuration is selected by validation accuracy; the final model is refit from scratch on the training split for 50 epochs.

### A.4 Harness Configuration

**Overview.** Each episode is executed by a Python orchestrator (orchestrator.py) that dispatches agent runs as isolated Apptainer container invocations. The container (agent.sif) packages a headless Chromium browser, the Playwright automation framework, and the MidScene PlaywrightAgent action loop. This design ensures that no browser state, cookies, or cached content persists across episodes or across agents.

**Episode execution.** For each (agent, question) pair, the orchestrator invokes the container with the agent’s API credentials, the task prompt, and a unique episode ID. Inside the container,

Hyperparameter	Value
Embedding dimension	16
Number of LSTM layers	2
Optimizer	Adam
Learning rate	$1 \times 10^{-3}$
Weight decay	$1 \times 10^{-4}$
Batch size	16
Epochs	50
Loss	Cross-entropy

Table 5: Fixed LSTM training hyperparameters.

Hyperparameter	Search space
Hidden dimension	64, 128, 256, 512
Dropout	0.2, 0.4

Table 6: LSTM grid search space ( $4 \times 2 = 8$  configurations, selected by validation accuracy).

`agent_runner.ts` navigates Chromium to the task start URL and runs `agent.aiAct(prompt)` until the task is complete or the per-episode timeout is reached. The browser viewport is fixed at  $1280 \times 768$  pixels across all agents and tasks. The MidScene replanning cycle limit is set to 40 across all agents, capping the maximum number of action–observation loops per episode.

**Event collection.** Browser interaction events are captured via two complementary paths to ensure completeness:

- **Primary (push bridge):** A `page_tracer.js` init script is injected into every page context. It patches the DOM event listeners and calls `window.__pushTraceEvent` for each recorded interaction (click, keydown, scroll, navigate, beforeunload, focus). Playwright routes these calls over the Chrome DevTools Protocol (CDP) to a host-side handler, which timestamps each event relative to the episode wall-clock start and appends it to the episode buffer. No polling is required.
- **Secondary (backstop harvest):** A single `harvest()` call at episode end reads any events remaining in the in-page `__agentTrace.events` array that did not complete their CDP bridge call before page teardown (most commonly `beforeunload` events mid-navigation).

HTTP-level page navigations — invisible to the in-page tracer — are captured separately via Playwright’s `framenavigated` listener and appended as `navigate` events with a `trigger: "http"` field.

**Output format.** Each completed episode is written as a JSON file at:

```
traces/{agent_id}/{dataset_name}/{timestamp}/{episode_id}.json
```

The file contains episode metadata (agent ID, model name, task type, timestamp), the agent’s answer and optional verification result, the MidScene action log, and the full DOM event trace including all timestamped browser interactions.

**Run configuration.** Experiments are specified via YAML configuration files that define the agent set, dataset slices, and run parameters. Table 7 summarises the fixed run parameters used across all experiments reported in this paper. Collecting traces for all datasets takes approximately three days. The cost of generating text for API accessed models totals USD 2890. The API’s used are provided by Anthropic, OpenAI and OpenRouter.

Parameter	Value
Browser	Chromium (headless)
Viewport	1280 × 768 px
Agent framework	MidScene PlaywrightAgent
Replanning cycle limit	40
Episodes per (agent, question)	1
Per-episode timeout	300 s
Parallel workers	5
Container runtime	Apptainer

Table 7: Fixed harness parameters used in all experiments.

## A.5 Behavioural Features Collected

For each browsing episode, we extract a fixed-dimensional feature vector from the client-side event trace. Let an episode consist of an ordered sequence of DOM events

$$E = \{e_1, e_2, \dots, e_T\},$$

where each event has a type (e.g., click, scroll, navigate), a timestamp, and optionally additional fields such as URL, scroll percentage, or screen coordinates. We also use the corresponding Midscene action log, which records the high-level actions issued by the agent through the browser harness.

We group features into five families: temporal dynamics, scrolling behaviour, click behaviour, navigation and action volume, and page-level normalised statistics.

**Event subsets.** From the raw event sequence, we define the following subsets:

$$E_{\text{click}}, E_{\text{scroll}}, E_{\text{nav}}, E_{\text{keydown}}, E_{\text{beforeunload}}, E_{\text{focus}},$$

corresponding respectively to click, scroll, navigation, keydown, beforeunload, and focus events. Let  $M$  denote the Midscene action log for the same episode.

We define the page count  $P$  as the number of distinct pages visited in the episode, using the recorded page count when available and otherwise falling back to the number of unique URLs observed in the DOM trace.

**Temporal dynamics.** To characterise interaction rhythm, we extract the sequence of event timestamps

$$t_1, t_2, \dots, t_T,$$

and compute inter-event intervals

$$\Delta_i = t_{i+1} - t_i \quad \text{for } i = 1, \dots, T - 1.$$

**Behavioral Feature Set** We extract 41 scalar features from each episode’s browser event trace (DOM event log). Features are grouped into seven categories below. All features are computed purely from client-side browser events (click, keydown, scroll, navigate, beforeunload, focus) and require no access to model internals or outputs.

Feature	Description
<i>Event volume</i>	
n_clicks	Total number of click events
n_scrolls	Total number of scroll events
n_navigations	Total number of page navigation events
n_keydowns	Total number of keydown events
n_focus	Total number of input/textarea focus events
n_events_total	Total events across all types
page_count	Number of distinct pages visited

n_unique_domains	Number of unique hostnames visited
<i>Global timing</i>	
total_duration_s	Wall-clock episode duration (seconds)
t_first_action_ms	Time from episode start to first event (ms)
mean_iei_ms	Mean inter-event interval across all events (ms)
std_iei_ms	Standard deviation of inter-event intervals (ms)
median_iei_ms	Median inter-event interval (ms)
p10_iei_ms	10th percentile inter-event interval (ms)
p90_iei_ms	90th percentile inter-event interval (ms)
iei_trend	Ratio of mean IEI in the second half of the episode to the first half; values > 1 indicate the agent slows down as context grows
<i>Per-type planning latency</i>	
mean_click_iei_ms	Mean inter-click interval (ms)
std_click_iei_ms	Std. of inter-click intervals (ms)
mean_nav_iei_ms	Mean inter-navigation interval, approximating page dwell time (ms)
std_nav_iei_ms	Std. of inter-navigation intervals (ms)
max_page_dwell_ms	Maximum single-page dwell time (ms)
mean_key_iei_ms	Mean inter-keydown interval, approximating API keystroke latency (ms)
std_key_iei_ms	Std. of inter-keydown intervals (ms)
<i>Scroll behavior</i>	
max_scroll_pct	Maximum scroll depth reached, as a percentage of page height
mean_scroll_pct	Mean scroll depth across all scroll events
n_deep_scrolls	Number of scroll events reaching >60% page depth
scroll_reversals	Number of direction reversals in the scroll depth sequence
<i>Click spatial distribution</i>	
click_x_std	Standard deviation of click <i>x</i> -coordinates (pixels)
click_y_std	Standard deviation of click <i>y</i> -coordinates (pixels)
click_bbox_area_frac	Bounding-box area of all click positions as a fraction of the 1280×768 viewport
click_top_frac	Fraction of clicks in the top quarter of the viewport ( <i>y</i> < 192px), capturing navbar/search-bar interaction
n_link_clicks	Number of clicks on anchor elements (href present)
link_click_ratio	$n\_link\_clicks / n\_clicks$
<i>Navigation strategy</i>	
popstate_ratio	Fraction of navigations triggered by popstate (history back)
scroll_to_click_ratio	$n\_scrolls / n\_clicks$
actions_per_page	$n\_events\_total / page\_count$
nav_to_click_ratio	$n\_navigations / n\_clicks$
keydowns_per_page	$n\_keydowns / page\_count$
focus_per_page	$n\_focus / page\_count$
structural_key_ratio	Fraction of keydowns that are structural keys (Enter, Arrow*, Tab, Escape, Backspace, Delete) vs. printable characters
<i>Exit behavior</i>	

mean\_exit\_scroll\_pct Mean scroll depth at beforeunload events, reflecting how far the agent had read before leaving each page

Table 8: The 41 behavioral features extracted from each episode trace

## B Supplementary Results

Table 9: Agent identification F1 (%) across datasets and classifiers. Best F1 per model group in **bold**. Macro f1 for each dataset and classifier is at the bottom of the table.

Model	Clf.	2Wiki (in-dom.)	FRAMES (in-dom.)	Webshop (in-dom.)	DeepShop (in-dom.)
<b>Proprietary Models</b>					
GPT-5.4	RF	85.71	72.19	68.09	66.67
	XGB	<b>91.50</b>	<b>78.48</b>	<b>68.78</b>	<b>68.29</b>
	LSTM	76.19	73.85	65.90	46.15
	Lasso	78.53	66.23	61.29	58.67
	LR	77.38	64.47	61.96	61.11
Claude Opus 4.6	RF	67.90	58.54	<b>67.13</b>	56.34
	XGB	<b>70.51</b>	<b>68.71</b>	66.18	<b>75.00</b>
	LSTM	46.51	58.03	57.14	48.72
	Lasso	52.11	59.67	55.81	57.83
	LR	47.89	60.34	56.49	60.24
Gemini-3.1-Pro	RF	64.75	64.86	<b>75.17</b>	52.05
	XGB	<b>65.19</b>	<b>75.16</b>	71.43	59.46
	LSTM	61.73	59.88	72.48	<b>61.11</b>
	Lasso	54.29	57.55	70.67	42.25
	LR	51.47	58.16	68.00	43.24
Gemini-3-Flash	RF	66.67	<b>54.01</b>	66.23	61.33
	XGB	<b>76.12</b>	52.70	<b>71.14</b>	<b>74.29</b>
	LSTM	67.53	49.18	56.16	55.88
	Lasso	67.10	37.18	59.15	46.58
	LR	67.53	40.26	59.57	43.24
Seed-2.0-Lite	RF	93.51	95.36	93.33	<b>90.24</b>
	XGB	<b>96.05</b>	96.60	93.42	87.50
	LSTM	87.90	<b>96.69</b>	<b>96.05</b>	90.14
	Lasso	89.47	87.84	95.17	86.42
	LR	92.62	87.84	95.17	85.00
<b>Open-Source Models</b>					
Gemma-4-31B-it	RF	80.26	73.68	73.55	53.16
	XGB	<b>82.12</b>	82.80	<b>74.17</b>	57.89
	LSTM	73.37	<b>84.77</b>	67.69	<b>63.41</b>
	Lasso	81.38	79.74	60.92	55.56
	LR	81.88	77.63	61.99	56.34
Gemma-4-26B	RF	69.92	48.65	61.64	30.19
	XGB	<b>72.87</b>	58.11	<b>72.26</b>	<b>57.58</b>
	LSTM	52.17	<b>64.38</b>	58.76	38.60
	Lasso	56.91	52.70	58.39	53.12
	LR	56.67	51.35	57.35	53.12
GLM-4.6V	RF	60.43	54.01	75.52	67.47
	XGB	<b>64.56</b>	<b>61.54</b>	79.45	<b>75.61</b>
	LSTM	38.46	48.18	<b>80.75</b>	67.57
	Lasso	53.59	56.00	77.50	62.50

Continued on next page

Table 9 – continued from previous page

Model	Clf.	2Wiki (in-dom.)	FRAMES (in-dom.)	Webshop (in-dom.)	DeepShop (in-dom.)
	LR	51.28	59.38	75.61	65.82
GLM-4.6V-Flash	RF	63.44	54.41	<b>54.10</b>	68.29
	XGB	70.86	65.28	45.38	<b>72.73</b>
	LSTM	<b>81.88</b>	<b>93.24</b>	35.59	60.24
	Lasso	56.25	57.33	24.24	59.52
	LR	57.67	56.38	27.27	56.47
Qwen3-VL-30B	RF	92.52	<b>81.82</b>	63.16	77.78
	XGB	<b>92.72</b>	80.27	<b>73.53</b>	<b>83.78</b>
	LSTM	88.61	79.75	57.72	61.11
	Lasso	85.16	70.00	56.58	70.13
	LR	87.01	70.89	59.21	69.23
Qwen3-VL-8B	RF	<b>82.61</b>	<b>83.45</b>	70.73	<b>68.42</b>
	XGB	<b>82.61</b>	81.38	<b>75.15</b>	<b>68.42</b>
	LSTM	67.20	74.45	57.99	40.54
	Lasso	66.67	68.57	51.85	44.78
	LR	68.09	70.42	51.09	41.18
Qwen3.5-27B	RF	84.15	94.94	80.56	86.49
	XGB	<b>90.91</b>	97.40	<b>82.19</b>	<b>87.67</b>
	LSTM	64.20	<b>98.67</b>	70.50	75.32
	Lasso	74.84	97.40	74.17	86.11
	LR	76.25	96.77	73.47	84.93
Qwen3.5-9B	RF	58.72	55.12	73.02	59.70
	XGB	<b>63.72</b>	<b>65.22</b>	<b>74.07</b>	<b>64.86</b>
	LSTM	38.98	56.29	58.16	50.49
	Lasso	42.11	48.12	60.87	59.74
	LR	44.64	48.89	59.57	60.53
UI-TARS-1.5-7B	RF	89.93	88.20	90.14	77.78
	XGB	<b>91.28</b>	<b>90.07</b>	<b>92.09</b>	<b>82.86</b>
	LSTM	89.80	86.71	77.04	74.29
	Lasso	84.00	70.44	75.18	71.43
	LR	86.11	72.96	75.18	72.46
<b>Macro F1 (14 models)</b>					
All	RF	75.75	69.95	72.31	65.42
	XGB	<b>79.36</b>	<b>75.27</b>	<b>74.23</b>	<b>72.57</b>
	LSTM	66.75	73.15	65.14	59.54
	Lasso	67.31	64.91	62.99	61.05
	LR	67.61	65.41	63.00	60.92

Table 10: OOD Per-Agent identification F1 (%) across datasets and classifiers. We report the Macro F1 for each classifier at the bottom. Best F1 per model group in **bold**

Model	Clf.	2Wiki→FRAMES (OOD)	FRAMES→2Wiki (OOD)	DeepShop→Webshop (OOD)	Webshop→DeepShop (OOD)
<b>Proprietary Models</b>					
GPT-5.4	RF	17.58	<b>51.11</b>	<b>65.53</b>	59.71
	XGB	17.02	50.97	60.43	<b>62.05</b>
	LSTM	<b>36.30</b>	39.74	48.05	60.34
Claude Opus 4.6	RF	23.24	31.47	<b>50.37</b>	37.91
	XGB	<b>26.87</b>	30.69	46.65	37.22
	LSTM	14.61	<b>35.04</b>	27.42	<b>38.50</b>
Gemini-3.1-Pro	RF	16.62	32.07	<b>58.89</b>	40.58
	XGB	21.23	34.66	57.05	38.77
	LSTM	<b>21.73</b>	<b>37.75</b>	54.11	<b>52.91</b>
Gemini-3-Flash	RF	36.96	<b>55.08</b>	39.95	40.49
	XGB	<b>37.78</b>	53.45	<b>52.85</b>	<b>53.39</b>
	LSTM	34.62	45.56	40.72	44.37
Seed-2.0-Lite	RF	67.05	86.05	89.03	74.61
	XGB	69.79	<b>90.73</b>	<b>89.60</b>	<b>75.77</b>
	LSTM	<b>71.39</b>	84.73	48.80	73.74
<b>Open-Source Models</b>					
Gemma-4-31B-it	RF	49.01	42.11	46.89	44.84
	XGB	43.61	44.34	<b>48.26</b>	43.75
	LSTM	<b>52.37</b>	<b>51.94</b>	40.68	<b>52.57</b>
Gemma-4-26B	RF	35.19	51.39	21.34	25.00
	XGB	<b>35.77</b>	<b>55.26</b>	<b>28.51</b>	<b>35.78</b>
	LSTM	35.25	53.58	15.22	22.83
GLM-4.6V	RF	35.15	22.87	25.41	<b>65.08</b>
	XGB	<b>35.73</b>	<b>30.93</b>	<b>60.08</b>	64.80
	LSTM	34.61	21.56	19.23	43.65
GLM-4.6V-Flash	RF	41.16	48.18	<b>54.58</b>	<b>23.70</b>
	XGB	44.44	44.22	42.93	21.80
	LSTM	<b>80.13</b>	<b>80.89</b>	37.26	18.78
Qwen3-VL-30B	RF	67.11	75.37	44.16	55.32
	XGB	<b>67.34</b>	77.01	<b>49.28</b>	<b>60.50</b>
	LSTM	66.53	<b>77.44</b>	26.73	50.22
Qwen3-VL-8B	RF	<b>73.74</b>	59.96	55.16	60.06
	XGB	71.28	<b>64.73</b>	<b>57.34</b>	<b>64.90</b>
	LSTM	63.91	54.04	44.37	57.06
Qwen3.5-27B	RF	0.15	0.61	<b>64.68</b>	<b>63.09</b>
	XGB	1.86	0.62	63.22	57.14
	LSTM	<b>21.98</b>	<b>10.98</b>	28.13	41.57
Qwen3.5-9B	RF	30.81	36.59	40.36	32.84
	XGB	<b>31.25</b>	36.95	<b>44.09</b>	39.07
	LSTM	30.50	<b>38.81</b>	30.61	<b>47.55</b>
UI-TARS-1.5-7B	RF	<b>74.72</b>	84.05	80.29	80.81
	XGB	71.05	82.12	<b>81.82</b>	<b>83.15</b>
	LSTM	70.06	<b>85.62</b>	77.44	79.42
<b>All Models (Macro F1)</b>					
All	RF	40.61	48.35	52.62	50.29
	XGB	41.07	49.76	<b>55.87</b>	<b>52.72</b>
	LSTM	<b>45.28</b>	<b>51.26</b>	38.48	48.82

Table 11: **Model families are also highly identifiable from their action traces.** There is a slight increase in overall performance for our XGBoost classifier when predicting by model families.

<b>Family</b>	<b>2Wiki</b>	<b>FRAMES</b>	<b>WebShop</b>	<b>DeepShop</b>
Seed-2	95.3	95.9	93.9	87.2
GPT-5	90.2	80.8	74.4	69.1
Claude 4	64.4	65.8	67.2	73.5
Gemini-3	68.2	72.5	75.2	60.9
Gemini-3-Flash	77.2	52.4	71.8	68.5
Gemma-4	86.5	77.6	76.7	69.9
GLM-4.6V	68.4	75.9	67.1	71.0
Qwen3-VL	90.7	94.7	91.3	87.3
Qwen3.5	75.4	76.6	79.6	76.4
UI-TARS-1.5	93.0	91.9	90.5	79.4
<b>All (weighted)</b>	<b>80.7</b>	<b>76.6</b>	<b>77.6</b>	<b>74.8</b>

Table 12: **Agent identifiability at both the model and family level.** Macro F1 for agent identification across 2Wiki, FRAMES, WebShop, and DeepShop. *Shaded header rows* show family-level classification (10-way); indented rows show individual-model classification (14-way). Each cell reports the best score across classifiers (RF, XGB, LSTM, Lasso, LR), with heat shading encoding value. Bottom row: weighted-average F1 (best classifier: XGB in all).

<b>Model</b>	<b>2Wiki</b>	<b>FRAMES</b>	<b>WebShop</b>	<b>DeepShop</b>
<b>Seed-2 (family)</b>	95.3	95.9	93.9	87.2
Seed-2.0-Lite	96.1	96.7	96.1	90.2
<b>GPT-5 (family)</b>	90.2	80.8	74.4	69.1
GPT-5.4	91.5	78.5	68.8	68.3
<b>Claude 4 (family)</b>	64.4	65.8	67.2	73.5
Claude Opus 4.6	70.5	68.7	67.1	75.0
<b>Gemini-3 (family)</b>	68.2	72.5	75.2	60.9
Gemini-3.1-Pro	65.2	75.2	75.2	61.1
<b>Gemini-3-Flash (family)</b>	77.2	52.4	71.8	68.5
Gemini-3-Flash	76.1	54.0	71.1	74.3
<b>Gemma-4 (family)</b>	86.5	77.6	76.7	69.9
Gemma-4-31B-it	82.1	84.8	74.2	63.4
Gemma-4-26B	72.9	64.4	72.3	57.6
<b>GLM-4.6V (family)</b>	68.4	75.9	67.1	71.0
GLM-4.6V	64.6	61.5	80.8	75.6
GLM-4.6V-Flash	81.9	93.2	54.1	72.7
<b>Qwen3-VL (family)</b>	90.7	94.7	91.3	87.3
Qwen3-VL-30B	92.7	81.8	73.5	83.8
Qwen3-VL-8B	82.6	83.5	75.2	68.4
<b>Qwen3.5 (family)</b>	75.4	76.6	79.6	76.4
Qwen3.5-27B	90.9	98.7	82.2	87.7
Qwen3.5-9B	63.7	65.2	74.1	64.9
<b>UI-TARS-1.5 (family)</b>	93.0	91.9	90.5	79.4
UI-TARS-1.5-7B	91.3	90.1	92.1	82.9
<b>All – family (weighted)</b>	80.7	76.6	77.6	74.8
<b>All – model (weighted)</b>	79.4	75.3	74.2	72.6

### B.1 Does Task Capability Predict Identifiability?

A central premise of our work is that each agent produces behaviourally distinct traces that are identifiable. A natural question is whether these traces are simply a proxy for task capability: if agents of similar capability tend to generate similar behavioural traces, our classifiers would be grouping agents by capability rather than recognising individual identity, and we would expect a significant correlation between task accuracy and identifiability. We explore this by examining whether such a correlation exists.

We measure capability as each agent’s accuracy on FRAMES[33]. Each agent is given a maximum of 40 turns to attempt each of the 75 questions in the test set. We evaluate the agent’s final response using an LLM-as-a-judge setup with gpt-5.4-mini, following the procedure described by Krishna et al. [33]; the evaluation prompt is provided below. Questions for which an agent failed to return a response within 40 turns are marked as incorrect; Table 13 reports completion counts per agent. We pair each agent’s accuracy with its identifiability, defined as the macro-averaged  $F_1$  of the best-performing classifier (XGBoost) in the closed-set fingerprinting setting, and compute both Pearson’s  $r$  and Spearman’s  $\rho$  across all 14 agents.

Figure 7 shows no meaningful relationship between the capability and identifiability. Neither correlation reaches statistical significance: Pearson’s  $r = 0.14$  ( $p = 0.626$ ) and Spearman’s  $\rho = 0.05$  ( $p = 0.852$ ). Agents span the full range of identifiability regardless of their accuracy: Claude Opus 4.6 achieves the highest accuracy (0.88) with moderate identifiability ( $F_1 = 0.69$ ), while UiTars-7B is among the most identifiable agents ( $F_1 = 0.90$ ) yet records the lowest accuracy (0.03).

This supports the view that each agent carries a distinctive behavioural fingerprint, shaped by how it sequences actions, manages tool calls, and navigates pages, that is orthogonal to its task performance. Agents do not converge on shared patterns simply because they perform similarly; rather, behavioural identity persists across the capability spectrum.

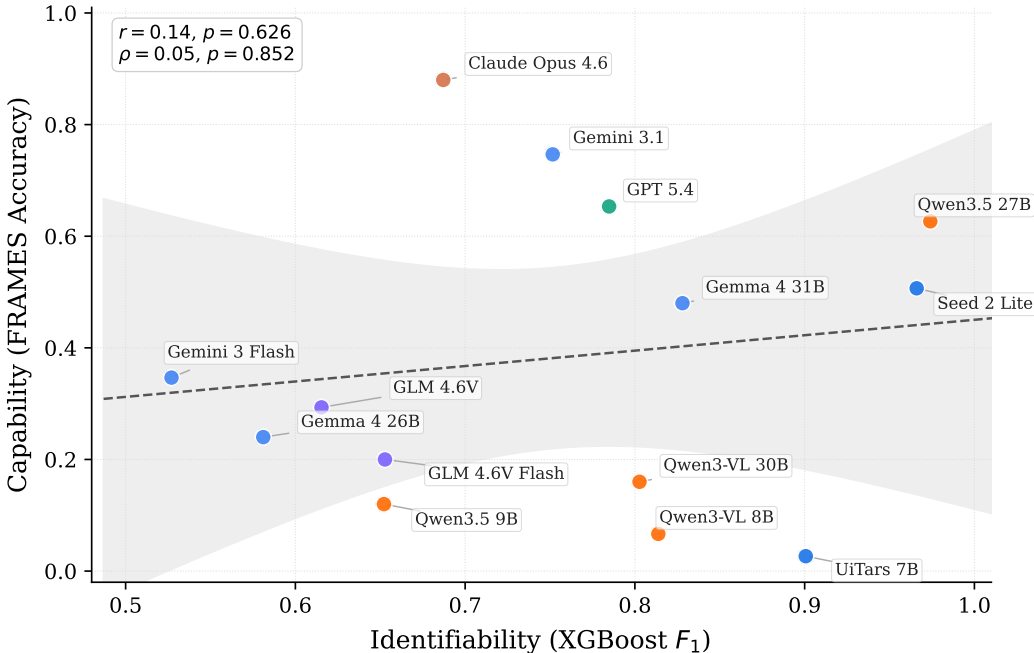


Figure 7: **Task capability does not predict agent identifiability.** Each point represents one of the 14 agents, with identifiability (XGBoost macro  $F_1$  in the closed-set setting) on the  $x$ -axis and task capability (accuracy on FRAMES) on the  $y$ -axis. The dashed line shows the linear regression fit with its 95% confidence band. Neither Pearson’s  $r = 0.14$  ( $p = 0.626$ ) nor Spearman’s  $\rho = 0.05$  ( $p = 0.852$ ) is statistically significant, indicating that the behavioural signatures that make an agent identifiable are largely orthogonal to its task capability.

Table 13: Agent completion counts, penalised accuracy, and closed-set identifiability (XGBoost  $F_1$ ) on the FRAMES test set (75 questions, 40-turn limit). Accuracy treats incomplete questions as incorrect. **Bold** denotes the highest value in each column.

Agent	Completed	Accuracy (%)	Ident. $F_1$ (%)
Claude Opus 4.6	72	<b>88.00</b>	68.71
Gemini 3.1	64	74.67	75.16
GPT-5.4	<b>75</b>	65.33	78.48
Qwen3.5-27B	54	62.67	<b>97.40</b>
Seed 2 Lite	50	50.67	96.60
Gemma-4-31B-it	58	48.00	82.80
Gemini 3 Flash	27	34.67	52.70
GLM-4.6V	46	29.33	61.54
Gemma-4-26B-A4B-it	26	24.00	58.11
GLM-4.6V Flash	39	20.00	65.28
Qwen3-VL-30B-A3B	35	16.00	80.27
Qwen3.5-9B	25	12.00	65.22
Qwen3-VL-8B	17	6.67	81.38
UITars-7B	10	2.67	90.07

### Automating Prompt

#### ===Task===

I need your help in evaluating an answer provided by an LLM against a ground truth answer. Your task is to determine if the ground truth answer is present in the LLM's response. Please analyze the provided data and make a decision.

#### ===Instructions===

1. Carefully compare the "Predicted Answer" with the "Ground Truth Answer".
2. Consider the substance of the answers – look for equivalent information or correct answers. Do not focus on exact wording unless the exact wording is crucial to the meaning.
3. Your final decision should be based on whether the meaning and the vital facts of the "Ground Truth Answer" are present in the "Predicted Answer".

#### ===Input Data===

- Question: {question}
- Predicted Answer: {LLM\_response}
- Ground Truth Answer: {ground\_truth\_answer}

#### ===Output Format===

Provide your final evaluation in the following format:

"Explanation:" (How you made the decision?)

"Decision:" ("TRUE" or "FALSE")

Please proceed with the evaluation.

## B.2 How well do our classifiers transfer across tasks and websites?

The main paper reports in-domain attribution, where train and test traces come from the same task distribution. Here we ask how far these fingerprints transfer across task and website boundaries. We compare three regimes: cross-task transfer, where a classifier is trained on one task and evaluated on another task hosted on the same website; pooled-site training, where traces from multiple tasks on the same website are combined before testing on each held-out test set; and cross-site transfer, where a classifier trained on one website is evaluated on another.

Train	Test	Website	Setting	Macro F1
2WikiMultiHopQA	2WikiMultiHopQA	Wikipedia	in-domain	79.4
FRAMES	FRAMES	Wikipedia	in-domain	75.3
WebShop	WebShop	Amazon	in-domain	74.3
DeepShop	DeepShop	Amazon	in-domain	72.6
2WikiMultiHopQA	FRAMES	Wikipedia	cross-task	41.1
FRAMES	2WikiMultiHopQA	Wikipedia	cross-task	49.8
2WikiMultiHopQA + FRAMES	2WikiMultiHopQA test	Wikipedia	pooled-site	81.3
2WikiMultiHopQA + FRAMES	FRAMES test	Wikipedia	pooled-site	77.2
WebShop	DeepShop	Amazon	cross-benchmark	52.7
DeepShop	WebShop	Amazon	cross-benchmark	55.9
WebShop + DeepShop	WebShop test	Amazon	pooled-site	78.8
WebShop + DeepShop	DeepShop test	Amazon	pooled-site	70.9
Wikipedia pooled	Amazon test	cross-site	cross-site	29.70
Amazon pooled	Wikipedia test	cross-site	cross-site	25.98

Table 14: **Training on diverse varied behaviours increases classifier performance.** We present generalisation results across task and website boundaries. Single-task transfer across tasks on the same site is substantially weaker than in-domain attribution, but pooling multiple tasks from the same website recovers strong performance. Cross-site transfer remains weak, suggesting that behavioural fingerprints are site-conditioned rather than universal.

The results in Table 14 show that behavioural fingerprints are not universal task-invariant signatures. Training on one Wikipedia task and testing on the other yields much weaker attribution than in-domain training, with macro F1 dropping from 79.4/75.3 in-domain to 41.1 and 49.8 under cross-task transfer. However, pooling 2WikiMultiHopQA and FRAMES training traces recovers strong attribution on both held-out test sets, reaching 81.3 on 2WikiMultiHopQA and 77.2 on FRAMES. This suggests that a site operator does not need a fingerprint that transfers from a single task to all possible tasks. Instead, diverse traces collected on the same website are sufficient to learn a robust site-conditioned identifier. Cross-site transfer remains much weaker, indicating that the identifying signal is shaped by the interaction between the model, task distribution, harness, and website interface.

### B.3 Which features are important to our classifiers ?

